Broad-Band Microwave Characterization of a Tri-Layer Structure Using a Coaxial Discontinuity with Applications for Magnetic Liquids and Films

Nour-eddine Belhadj-Tahar, Olivier Dubrunfaut, and Arlette Fourrier-Lamer

***Abstract*—An analytic technique is described, which allows us to determine simultaneously complex permittivity ε and permeability μ of magnetic films or magnetic liquids. The cell is a gap in a coaxial line filled with three layers (for liquid samples, the two external layers are used as windows, and for films, the middle layer constitutes the substrate). Permittivity and permeability of the unknown layer(s) are computed from the S-parameters (S_{11}, S_{21}), which are measured on the gap, taking into account higher order modes excited at the discontinuity. ε and μ measured for ethanol and a ferrofluid (with an applied magnetic static field) are presented up to 18 GHz.**

***Index Terms*—Broad-band measurements, coaxial discontinuity, ferrofluid, magnetic film, microwave characterization, mode-matching method, permeability, permittivity, tri-layer.**

I. Introduction

MICROWAVE applications connected with magnetic liquids (modulator, absorber) and magnetic films (microwave components) require the development of appropriate characterization methods. To this end, we propose a broad-band method for simultaneous measurement of permittivity and permeability using a circular waveguide as a coaxial discontinuity. This kind of cell has already been used in different configurations: reflection measurements appropriated for dielectric material characterization (solid [1] or liquid [2]) and reflection/transmission measurements for magnetic solid-material characterization [3] or dielectric materials with a permittivity tensor [4]. Here, the cell is composed of three layers (either an airtight cell or a middle substrate with films) with the cell inserted between two coaxial guides, the transmission (S_{21}) and reflection (S_{11}) coefficients are measured with a network analyzer; the permittivity and permeability of the unknown layer(s) are then computed.

A comparable method where the cell is a coaxial guide is widely used for broad-band measurements [5]. It is easily adaptable to bi- or tri-layer. With this method, the increase in frequency is limited by the appearance of resonance phenomena due to the cell length.

Manuscript received February 13, 1998; revised July 1, 1998.

The authors are with the Laboratoire de Dispositifs Infrarouge et Micro-ondes (LDIM), Université Pierre et Marie Curie, 75252 Paris, France (e-mail: nebt@ccr.jussieu.fr).

Publisher Item Identifier S 0018-9480(98)09062-0.

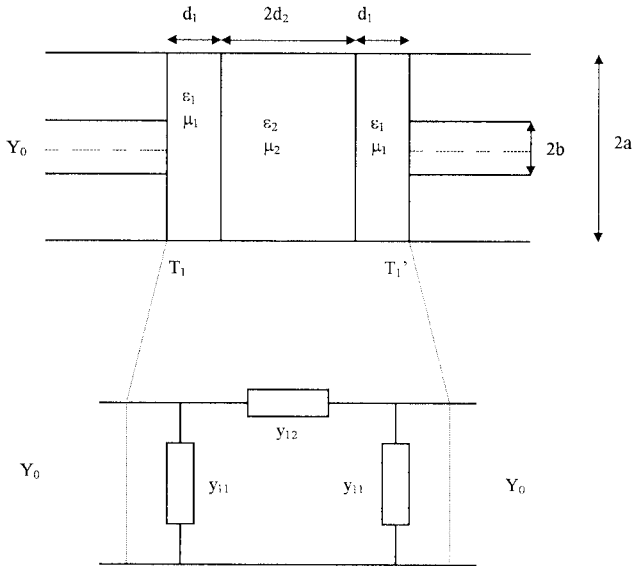

Fig. 1. Geometry of the structure and an equivalent representation.

We present the direct problem first, and then the inverse one. Some experimental results illustrate the method.

II. Direct Problem

The proposed structure is depicted in Fig. 1. The coaxial air line is interrupted by a circular waveguide formed by three layers. The symmetry of the cell is needed to solve simply the electromagnetic problem. The two materials forming the tri-layer are assumed to be homogeneous and isotropic: $(\varepsilon_1 = \varepsilon_1' - j\varepsilon_1''; \mu_1 = \mu_1' - j\mu_1'')$ and $(\varepsilon_2 = \varepsilon_2' - j\varepsilon_2''; \mu_2 = \mu_2' - j\mu_2'')$ are, respectively, the relative permittivity and permeability of the extern and middle layers.

A. Theoretical Resolution

We must express the S-parameters as functions of $(\varepsilon_1; \mu_1)$ and $(\varepsilon_2; \mu_2)$, assuming that the coaxial line propagates the TEM mode only. The structure between planes T_1 and T_1' can be represented as a quadripole characterized by its $[Y]$ matrix; the admittances are normalized in relation to the characteristic

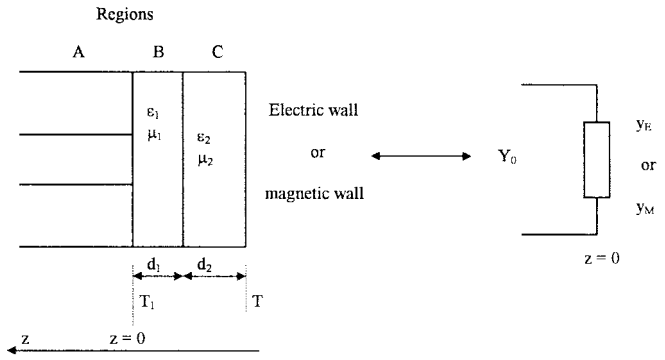

Fig. 2. Representation of the bisected structure.

admittance Y_0 of the coaxial line. The relationships between $[Y]$ and the S-parameters are trivial

$$S_{11} = S_{22} = \frac{1 - y_{11}(y_{11} + 2y_{12})}{(1 + y_{11})(1 + y_{11} + 2y_{12})} \tag{1}$$

$$S_{21} = S_{12} = \frac{2y_{12}}{(1 + y_{11})(1 + y_{11} + 2y_{12})}. \tag{2}$$

Let us apply the bisection theorem. In the presence of an electric wall placed at plane T, the normalized input admittance at plane T_1 is from Fig. 2, as follows:

$$y_E = y_{11} + 2y_{12}. \tag{3}$$

If a magnetic wall is then placed at plane T, the input admittance at plane T_1 becomes

$$y_M = y_{11}. \tag{4}$$

As a result, (1) and (2) can be written as

$$S_{11} = S_{22} = \frac{1 - y_M y_E}{(1 + y_M)(1 + y_E)} \tag{5}$$

$$S_{21} = S_{12} = \frac{y_E - y_M}{(1 + y_M)(1 + y_E)}. \tag{6}$$

Thus, in order to solve the reflection/transmission problem, we have to express y_E and y_M (bi-layer in reflection) as functions of (ε_1, μ_1) and (ε_2, μ_2).

The TEM mode excites an infinite number of TM_{0i} modes at the geometrical discontinuity. The electromagnetic problem is solved by matching the fields at the interfaces of the layered materials and using the orthogonality properties of modes in cylindrical waveguides. The electric-wall case has already been presented for a dielectric material [2]. For a magnetic material, we only have to add the term of permeability in the expression of the propagation constant in free space k_i ($k_i^2 = k_0^2 \varepsilon_i \mu_i$ with $i = 1$ or 2 and $k_0 = \omega\sqrt{\varepsilon_0 \mu_0}$ where ε_0 and μ_0 are the permittivity and permeability of vacuum and $\omega = 2\pi f$, f is the operating frequency).

We find for a cell ended with an electric wall (as shown in Appendix A)

$$y_E = j\frac{2k_0 a \varepsilon_1}{\ln\left(\frac{a}{b}\right)}\left(y_0 - \sum_{m=1}^{\infty} x_m y_m\right) \tag{7}$$

where y_0 and y_m are determinate as follows:

$$y_0 = \sum_{n=1}^{\infty} \frac{1 - \Gamma_n}{1 + \Gamma_n} \frac{1}{\lambda_n^2 a^2 \sqrt{\lambda_n^2 a^2 - k_0^2 a^2 \varepsilon_1 \mu_1}} \frac{J_0^2(\lambda_n b)}{J_1^2(\lambda_n a)} \tag{8}$$

$$y_m = -\sum_{n=1}^{\infty} \frac{1 - \Gamma_n}{1 + \Gamma_n} \frac{1}{(\lambda_n^2 a^2 - \pi_m^2 a^2)\sqrt{\lambda_n^2 a^2 - k_0^2 a^2 \varepsilon_1 \mu_1}} \cdot \frac{J_0^2(\lambda_n b)}{J_1^2(\lambda_n a)} \tag{9}$$

with Γ_n given by (10), shown at the bottom of this page, and x_m is calculated by resolving the system

$$\sum_{m=1}^{\infty} A_{mq} x_m = y_q, \qquad q = 1, 2, \cdots \tag{11}$$

where

$$A_{mq} = \frac{\lambda_n^2 a^2}{(\lambda_n^2 a^2 - \pi_q^2 a^2)(\lambda_n^2 a^2 - \pi_m^2 a^2)\sqrt{\lambda_n^2 a^2 - k_0^2 \varepsilon_1 \mu_1 a^2}} \cdot \frac{1 - \Gamma_n}{1 + \Gamma_n} \frac{J_0^2(\lambda_n b)}{J_1^2(\lambda_n a)} + \frac{1}{\varepsilon_1} \frac{\delta_{mq}}{4\sqrt{\pi_q^2 a^2 - k_0^2 a^2}} \cdot \left[\frac{a^2 Z_1^2(\pi_q a)}{b^2 Z_1^2(\pi_q b)} - 1\right]. \tag{12}$$

In (7)–(12), δ_{mq} is the Kronecker delta function, J_0 and J_1 are, respectively, the zeroth- and first-order Bessel functions of the first kind and Z_1 represents the linear combination as follows:

$$Z_1(s) = J_1(s) - \frac{J_0(s)}{N_0(s)} N_1(s) \tag{13}$$

where N_i is the ith-order Bessel function of the second kind; λ_n are computed by solving the equation

$$J_0(\lambda_n a) = 0, \qquad n = 1, 2, \cdots \tag{14}$$

and π_i by solving the equation

$$J_0(\pi_i a) N_0(\pi_i b) - J_0(\pi_i b) N_0(\pi_i a) = 0, \qquad i = 1, 2, \cdots. \tag{15}$$

We find the same results for y_M (with a magnetic wall placed at plane T) by substituting coth function with tanh function in (10).

$$\Gamma_n = \frac{\dfrac{\varepsilon_1}{\sqrt{\lambda_n^2 - k_0^2 \varepsilon_1 \mu_1}} - \dfrac{\varepsilon_2}{\sqrt{\lambda_n^2 - k_0^2 \varepsilon_2 \mu_2}} \coth\left(d_2 \sqrt{\lambda_n^2 - k_0^2 \varepsilon_2 \mu_2}\right)}{\dfrac{\varepsilon_1}{\sqrt{\lambda_n^2 - k_0^2 \varepsilon_1 \mu_1}} + \dfrac{\varepsilon_2}{\sqrt{\lambda_n^2 - k_0^2 \varepsilon_2 \mu_2}} \coth\left(d_2 \sqrt{\lambda_n^2 - k_0^2 \varepsilon_2 \mu_2}\right)} \exp\left(-2d_1 \sqrt{\lambda_n^2 - k_0^2 \varepsilon_1 \mu_1}\right) \tag{10}$$

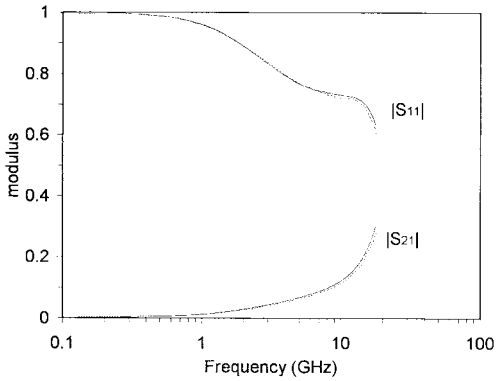

(a)

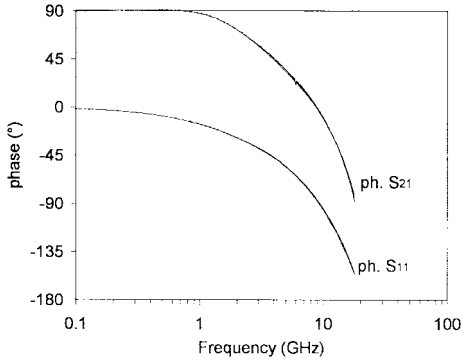

(b)

Fig. 3. Measured (- - -) and calculated (——) S-parameters of a tri-layered structure formed by Altuglass windows ($d_1 = 0.5$ mm) and ethanol ($2d_2 = 3.2$ mm) in APC-7-mm standard. (a) Modulus. (b) Phase.

B. Numerical Computation and Experimental Results

For numerical computation, the number of TM_{0m} modes in the coaxial line (M) and of TM_{0n} modes in the tri-layer structure (N) must be fixed: the infinite series [(7)–(9) and (11)–(12)] are truncated. It has been showed that $M = 3$ and $N = 6$ give a sufficient numerical accuracy compared to a measurement one [2].

The airtight cell configuration is now tested using an APC-7-mm standard air line. The structure is formed by two Altuglass windows ($d_1 = 0.5$ mm) and ethanol ($2d_2 = 3.2$ mm). Altuglass permittivity is first determined by the method where the cell is a circular waveguide measuring in reflection [1] ($\mu_1 = 1$; $\varepsilon_1 \approx 2.6 - j0.1$ between 45 MHz and 18 GHz). The dielectric properties of ethanol at 20 °C are summarized from [6] by

$$\varepsilon_2(\omega) = \varepsilon_\infty + \frac{\varepsilon_s - \varepsilon_\infty}{1 + j\dfrac{\omega}{\omega_0}} \tag{16}$$

where $\varepsilon_\infty = 4.2$, $\varepsilon_S = 25.07, (\omega_0/2\pi) = 1.1$ GHz. Knowing the constitutive parameters of the three layers, the S-parameters measured and calculated are compared in Fig. 3. These results show a good agreement.

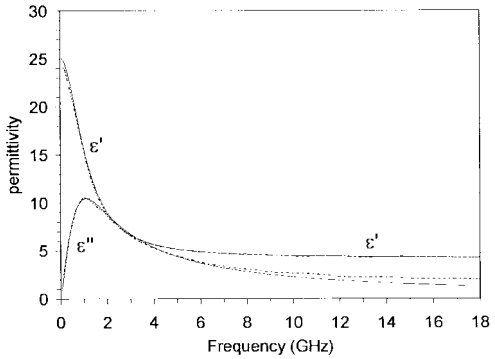

Fig. 4. Complex permittivity of ethanol measured in the tight tri-layered structure formed by Altuglass windows ($d_1 = 0.5$ mm) and ethanol ($2d_2 = 3.2$ mm) in APC-7-mm standard (- - -) and theoretical law (——).

III. Inverse Problem: Accuracy and Experimental Results

An iterative method is used to calculate ε_i and μ_i, the constitutive parameters of the unknown layer, from the S-parameters (cf. Appendix B for details). Here, we discuss results for the airtight cell configuration. The cell characteristics (thickness, ε_1, μ_1) are optimized to have the best sensitivity on (ε_2, μ_2) next to the S-parameters [7]. Nevertheless the accuracy on the permeability is bad at low frequencies. Indeed, the liquid permeability μ_2 only appears in y_E and y_M expressions in the term [cf. (10)]

$$\sqrt{\lambda_n^2 - k_0^2 \varepsilon_2 \mu_2}. \tag{17}$$

Thus, when $k_0^2|\varepsilon_2\mu_2|$ is negligible compared with the lowest λ_n, i.e., λ_1, accuracy on μ_2 is not good enough. In practice, the accuracy is better than 5% with an HP 8510 if

$$k_0^2|\varepsilon_2\mu_2| > \frac{\lambda_1^2}{10}. \tag{18}$$

From (14), the first zero is

$$\lambda_1 a = 2.405. \tag{19}$$

From (18) and (19), the accuracy condition on μ_2 can be written as

$$f_{\mathrm{GHz}} > \frac{40}{a_{mm}\sqrt{|\varepsilon_2\mu_2|}}. \tag{20}$$

Furthermore, the loss tangents $\varepsilon_2''/\varepsilon_2'$ and μ_2''/μ_2' should be greater than 0.01 to have a reasonable accuracy on ε_2'' and μ_2'' (better than 5%).

Measurements are obtained at 20 °C using the HP8510B network analyzer in a APC-7-mm standard air line. At first, we present results on ethanol used as a dielectric standard [with the law reminded at (16)]. The theoretical and measured results compared in Fig. 4 for permittivity are in a good agreement. Concerning permeability, measurements shown in Fig. 5 are accurate above 4 GHz in accordance with (20).

As an example, the method is used with an appropriate material: a magnetic liquid, namely, a ferrofluid. A static magnetic field parallel to the cell axis is added. Ferrofluids

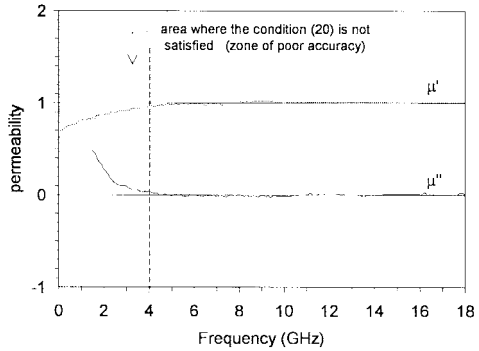

Fig. 5. Complex permeability of ethanol measured in the tight tri-layered structure formed by Altuglass windows ($d_1 = 0.5$ mm) and ethanol ($2d_2 = 3.2$ mm) in APC-7-mm standard.

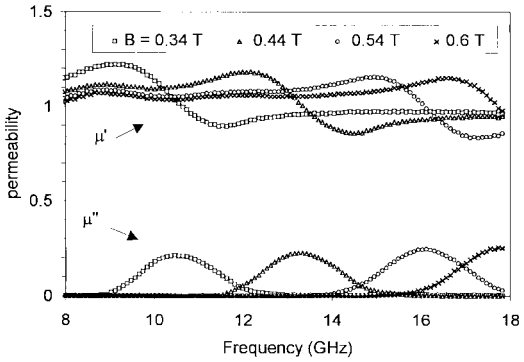

Fig. 6. Complex permeability of a ferrofluid (Fe_2MnO_4 in CCl_4 mixed with ethanol) measured in the tight trilayered structure formed by Altuglass windows ($d_1 = 0.5$ mm) and ferrofluid ($2d_2 = 3.2$ mm) in APC-7-mm standard with different static magnetic field.

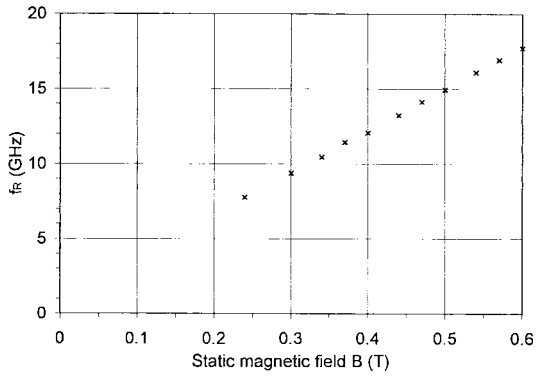

Fig. 7. Variation of the magnetic resonance frequency for a ferrofluid (Fe_2MnO_4 in CCl_4 mixed with ethanol) with the applied static magnetic field.

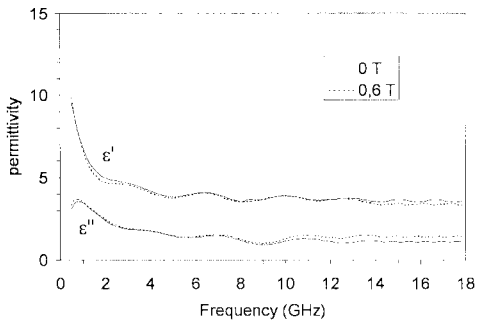

Fig. 8. Complex permittivity of a ferrofluid (Fe_2MnO_4 in CCl_4 mixed with ethanol) measured in the tight tri-layered structure formed by Altuglass windows ($d_1 = 0.5$ mm) and ferrofluid ($2d_2 = 3.2$ mm) in APC-7-mm standard with a 0.6-T static magnetic field and without static magnetic field.

are colloidal suspensions of magnetic particles in a carrier liquid. The samples we used were prepared in Laboratory LI2 (Paris VI) by the ionic method [8] using tetrachloride (mixed with ethanol) as carrier liquid and manganese ferrite particles (Fe_2MnO_4). They are spherical with an average diameter equal to 15 nm involving monodomain magnetic properties. Both the low volumic concentration (4.5%) and the surface ionization (the particles repel one another) involve that particle–particle magnetic interactions are negligible. Consequently, the frequency at resonance is given by Kittel's formula (case of a sphere) [9]

$$f_R = \gamma(B_A + B) \tag{21}$$

where γ is the gyromagnetic ratio taken as 28 GHz/T, B_A the anisotropy field and B the applied static magnetic field. Fig. 6 shows the permeability spectrum for different fields. We can see a resonance phenomena where the characteristic frequency is linearly dependent on B, as reported in Fig. 7, in accordance with the Kittel's formula. From this graph and (21), the gyromagnetic ratio computed is equal to 27.8 GHz/T (2%), close to the theoretical value.

Let's note that, due to the low permittivity of the solution (reported in Fig. 8, quasi-independent from the static magnetic field), the permeability accuracy is better than 5% only over 6 GHz, in accordance with (20).

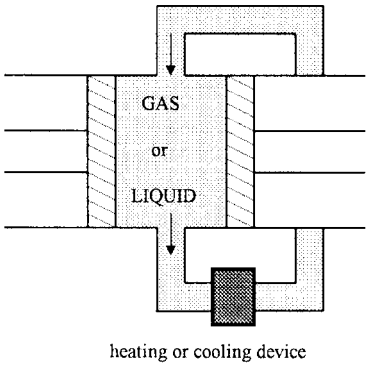

Fig. 9. Temperature measurement for a gas or liquid.

IV. Conclusion

In this paper, we have presented a broad-band method for measuring magnetic liquid. Measurements on ethanol and ferrofluid have shown its viability, with or without an applied magnetic field. Two kinds of experiments are presently envisaged with this cell; first, temperature variations of the material measured. Such a structure is particularly well adapted to this purpose, as described in Fig. 9. The gas or the liquid under test is heated or cooled with an outside device connected with

the cell by two ducts. The circulation ducts do not alter the electromagnetic configuration (if waves are not propagating in it) because of the low $|\vec{E}|$ and $|\vec{H}|$ near the lateral part of the cell. Moreover, the temperature variation do not affect calibration because of the windows (thermal insulator chosen) separating room temperature and coaxial waveguide. Second, magnetic film characterizations, the cell being formed by two identical films coating the sides of the middle layer used as a substrate.

APPENDIX A
DIRECT PROBLEM

The direct problem for the reflection/transmission structure involves the y_E and y_M (cf. Fig. 2) determination by a modal analysis combined with the mode-matching method.

The nature of the TEM mode and the cylindrical symmetry of Fig. 2 enable us to predict that only higher order modes of type TM independent of the azimuthal angle Φ are excited at the geometrical discontinuity plane T_1.

In the coaxial line (A region), the components of the total electromagnetic field are

$$E_{rA} = \frac{1}{r}A_0[\exp(jk_0z) + \Gamma\exp(-jk_0z)] + \sum_{m=1}^{\infty} A_m Z_1(\pi_m r)\exp(-\gamma_{Am}z) \quad \text{(A1)}$$

$$E_{zA} = \sum_{m=1}^{\infty} A_m \frac{\pi_m}{\gamma_{Am}} Z_0(\pi_m r)\exp(-\gamma_{AM}z) \quad \text{(A2)}$$

$$H_{\Phi A} = \frac{1}{r}A_0 Y_{A0}[\exp(jk_0z) - \Gamma\exp(-jk_0z)] + \sum_{m=1}^{\infty} A_m Y_{Am} Z_1(\pi_{Am}r)\exp(-\gamma_{Am}z) \quad \text{(A3)}$$

where a time dependence of $\exp(j\omega t)$ is assumed, with $\omega = 2\pi f$ and f the operating frequency. A_0 represents the incident TEM wave amplitude and Γ its reflection coefficient at plane T_1. Y_{A0} and Y_{Am} are, respectively, the wave admittances of the TEM and TM_{0m} in the coaxial waveguide

$$Y_{A0} = -\sqrt{\frac{\varepsilon_0}{\mu_0}} \quad \text{(A4)}$$

$$Y_{Am} = \frac{j\omega\varepsilon_0}{\gamma_{Am}} \quad \text{(A5)}$$

with ε_0 and μ_0 the permittivity and permeability of vacuum

$$k_0 = \omega\sqrt{\varepsilon_0\mu_0} \quad \text{(A6)}$$

and

$$\gamma_{Am} = \sqrt{\pi_m^2 - k_0^2}. \quad \text{(A7)}$$

In (A1)–(A3), Z_i represents the linear combination of the ith-order Bessel functions of the first and second kinds as follows:

$$Z_i(\pi_m r) = J_i(\pi_m r) + G_{Am}N_i(\pi_m r). \quad \text{(A8)}$$

In the first layer (B region)

$$E_{rB} = \sum_{n=1}^{\infty} B_n J_1(\lambda_n r)[\exp(\gamma_{Bn}z) + \Gamma_n\exp(-\exp(-\gamma_{Bn}z)] \quad \text{(A9)}$$

$$E_{zB} = \sum_{n=1}^{\infty} B_n \frac{\lambda_n}{\gamma_{Bn}} J_0(\lambda_n r)[\exp(\gamma_{Bn}z) - \Gamma_n\exp(-\gamma_{Bn}z)] \quad \text{(A10)}$$

$$H_{\Phi B} = \sum_{n=1}^{\infty} Y_{Bn}B_n J_1(\lambda_n r)[\exp(\gamma_{Bn}z) - \Gamma_n\exp(-\gamma_{Bn}z)] \quad \text{(A11)}$$

where Γ_n represents the reflection coefficient of the TM_{0n} higher order mode in the first layer at plane T_1, and Y_{Bn} the admittance of this mode:

$$Y_{Bn} = -j\frac{\omega\varepsilon_0\varepsilon_1}{\gamma_{Bn}} \quad \text{(A12)}$$

with

$$\gamma_{Bn} = \sqrt{\lambda_n^2 - k_0^2\varepsilon_1\mu_1}. \quad \text{(A13)}$$

When an electric wall is placed at plane T, the electric-field boundary conditions at this plane provide the solutions for the second layer (C region)

$$E_{rC} = \sum_{p=1}^{\infty} C_p J_1(\chi_p r)sh[\gamma_{C_p}(z + d_1 + d_2)] \quad \text{(A14)}$$

$$E_{zC} = \sum_{p=1}^{\infty} C_p \frac{\chi_p}{\gamma_{C_p}} J_0(\chi_p r)ch[\gamma_{C_p}(z + d_1 + d_2)] \quad \text{(A15)}$$

$$H_{\Phi C} = \sum_{p=1}^{\infty} Y_{C_p}C_p J_1(\chi_p r)ch[\gamma_{C_p}(z + d_1 + d_2)] \quad \text{(A16)}$$

with

$$Y_{C_p} = -j\frac{\omega\varepsilon_0\varepsilon_2}{\gamma_{C_p}} \quad \text{(A17)}$$

and

$$\gamma_{C_p} = \sqrt{\chi_p^2 - k_0^2\varepsilon_2\mu_2}. \quad \text{(A18)}$$

The E_z axial component of the electrical field for each TM mode must be zero at the conductors in the three regions. The following conditions are thus obtained by canceling the relations (A2), (A10), and (A15):

$$Z_0(\pi_m a) = Z_0(\pi_m b) = 0 \quad \text{(A19)}$$

$$J_0(\lambda_n a) = 0 \quad \text{(A20)}$$

$$J_0(\chi_p a) = 0. \quad \text{(A21)}$$

Equation (A19) enables us to determine the coefficient G_{Am} contained in (A8)

$$G_{Am} = -\frac{J_0(\pi_m a)}{N_0(\pi_m a)} = -\frac{J_0(\pi_m b)}{N_0(\pi_m b)} \tag{A22}$$

and, thus, from the following transcendental equation, we obtain the coefficients π_m

$$J_0(\pi_m a)N_0(\pi_m b) - J_0(\pi_m b)N_0(\pi_m a) = 0. \tag{A23}$$

The constants λ_n and χ_p are obtained by solving (A20) and (A21). Note that λ_n and χ_p are equal for $n = p$.

From the relations (A9), (A11), (A1), and (A3), the boundary conditions for the transverse components at plane T_1 are written in the following manner:

$$E_{rB} = 0, \qquad 0 < r < b \tag{A24}$$

$$E_{rB} = \sum_{n=1}^{\infty} B_n J_1(\lambda_n r)[1+\Gamma_n] = \frac{1}{r}A_0[1+\Gamma] + \sum_{m=1}^{\infty} A_m Z_1(\pi_m r), \qquad b < r < a \tag{A25}$$

$$H_{\Phi B} = \sum_{n=1}^{\infty} Y_{Bn} B_n J_1(\lambda_n r)[1-\Gamma_n] = \frac{1}{r}A_0 Y_{A0}[1-\Gamma] + \sum_{m=1}^{\infty} A_m Y_{Am} Z_1(\pi_m r), \qquad b < r < a. \tag{A26}$$

The coefficients A_m and B_n are determined by using the orthogonality properties of Bessel functions.

The first step consists of performing the integrals $\int_0^a rJ_1(\lambda_n r)E_{rB}\,dr$. The substitution of E_{rB} from (A24) and (A25) in the above integral yields

$$\frac{B_n[1+\Gamma_n]}{\lambda_n} = A_0[1+\Gamma]\frac{2J_0(\lambda_n b)}{\lambda_n^2 a^2 J_1^2(\lambda_n a)} \cdot \left[1 - \sum_{m=1}^{\infty} \frac{A_m}{A_0(1+\Gamma)} \frac{bZ_1(\pi_m b)}{\frac{\pi_m^2}{\lambda_n^2} - 1}\right], \quad \text{for } n = 1, 2, 3, \cdots. \tag{A27}$$

Next, we integrate $H_{\Phi B}$ between $r = b$ and $r = a$. We obtain from (A26)

$$Y_{A0}A_0[1-\Gamma]\ln\left(\frac{a}{b}\right) = \sum_{n=1}^{\infty} \frac{Y_{Bn}B_n}{\lambda_n}[1-\Gamma_n]J_0(\lambda_n b). \tag{A28}$$

At plane T_1, the input admittance normalized in relation to the characteristic admittance of the coaxial waveguide is

$$y_E = \frac{1-\Gamma}{1+\Gamma} \tag{A29}$$

so (A27) and (A28) give us the following result:

$$y_E = j\frac{2k_0\varepsilon_1}{\ln\left(\frac{a}{b}\right)} \sum_{n=1}^{\infty} \cdot \frac{J_0^2(\lambda_n b)}{[\lambda_n^2 a^2 J_1^2(\lambda_n a)]\sqrt{\lambda_n^2 a^2 - k_0^2 a^2 \varepsilon_1 \mu_1}} \frac{1-\Gamma_n}{1+\Gamma_n} \cdot \left[1 - \sum_{m=1}^{\infty} \frac{A_m}{A_0(1+\Gamma)} \frac{bZ_1(\pi_m b)}{\frac{\pi_m^2}{\lambda_n^2} - 1}\right]. \tag{A30}$$

This may be written in the form

$$y_E = j\frac{2k_0 a\varepsilon_1}{\ln\left(\frac{a}{b}\right)}\left(y_0 - \sum_{m=1}^{\infty} x_m y_m\right) \tag{A31}$$

where y_0, x_m, and y_m are defined as

$$y_0 = \sum_{n=1}^{\infty} \frac{1-\Gamma_n}{1+\Gamma_n} \frac{1}{\lambda_n^2 a^2 \sqrt{\lambda_n^2 a^2 - k_0^2 a^2 \varepsilon_1 \mu_1}} \frac{J_0^2(\lambda_n b)}{J_1^2(\lambda_n a)} \tag{A32}$$

$$x_m = \frac{A_m}{A_0(1+\Gamma)} bZ_1(\pi_m b) \tag{A33}$$

$$y_m = -\sum_{n=1}^{\infty} \frac{1-\Gamma_n}{1+\Gamma_n} \frac{1}{(\lambda_n^2 a^2 - \pi_m^2 a^2)\sqrt{\lambda_n^2 a^2 - k_0^2 a^2 \varepsilon_1 \mu_1}} \cdot \frac{J_0^2(\lambda_n b)}{J_1^2(\lambda_n a)}. \tag{A34}$$

In (A31)–(A34), Γ_n and x_m are still unknown.

Γ_n is computed by using orthogonality properties of TM modes in the cylindrical waveguide. The total electromagnetic field in the B and C regions is matched at the plane $z = -d_1$. Referring to (A9), (A11), (A14), and (A16), we have

$$E_{rB} = \sum_{n=1}^{\infty} B_n J_1(\lambda_n r)[\exp(-\gamma_{Bn} d_1) + \Gamma_n \exp(\gamma_{Bn} d_1)] = \sum_{p=1}^{\infty} C_p J_1(\chi_p r) sh(\gamma_{C_p} d_2) \tag{A35}$$

$$H_{\Phi B} = \sum_{n=1}^{\infty} Y_{Bn} B_n J_1(\lambda_n r)[\exp(-\gamma_{Bn} d_1) - \Gamma_n \exp(\gamma_{Bn} d_1)] = \sum_{p=1}^{\infty} Y_{C_p} C_p J_1(\chi_p r) ch(\gamma_{C_p} d_2). \tag{A36}$$

The above relations are used to perform the integrals $\int_0^a rJ_1(\lambda_n r)E_{rB}dr$ and $\int_0^a rJ_1(\lambda_n r)H_{\Phi B}\,dr$. Integrating and using (A12) and (A17), we may write

$$B_n[\exp(-\gamma_{Bn} d_1) + \Gamma_n \exp(\gamma_{Bn} d_1)] = C_p sh(\gamma_{C_p} d_2), \qquad \text{for } n = p \tag{A37}$$

$$\frac{\varepsilon_1}{\gamma_{Bn}} B_n[\exp(-\gamma_{Bn} d_1) - \Gamma_n \exp(\gamma_{Bn} d_1)] = \frac{\varepsilon_2}{\gamma_{C_p}} C_p ch(\gamma_{C_p} d_2), \qquad \text{for } n = p \tag{A38}$$

$$\Gamma_n = \frac{\dfrac{\varepsilon_1}{\sqrt{\lambda_n^2 - k_0^2\varepsilon_1\mu_1}} - \dfrac{\varepsilon_2}{\sqrt{\lambda_n^2 - k_0^2\varepsilon_2\mu_2}}\coth\left(d_2\sqrt{\lambda_n^2 - k_0^2\varepsilon_2\mu_2}\right)}{\dfrac{\varepsilon_1}{\sqrt{\lambda_n^2 - k_0^2\varepsilon_1\mu_1}} + \dfrac{\varepsilon_2}{\sqrt{\lambda_n^2 - k_0^2\varepsilon_2\mu_2}}\coth\left(d_2\sqrt{\lambda_n^2 - k_0^2\varepsilon_2\mu_2}\right)}\exp\left(-2d_1\sqrt{\lambda_n^2 - k_0^2\varepsilon_1\mu_1}\right) \tag{A42}$$

$$A_{mq} = \sum_{n=1}^{\infty}\frac{\lambda_n^2 a^2}{(\lambda_n^2a^2 - \pi_q^2a^2)(\lambda_n^2a^2 - \pi_m^2a^2)\sqrt{\lambda_n^2a^2 - k_0^2\varepsilon_1\mu_1a^2}}\frac{1-\Gamma_n}{1+\Gamma_n}\frac{J_0^2(\lambda_n b)}{J_1^2(\lambda_n a)} + \frac{1}{\varepsilon_1}\frac{\delta_{mq}}{4\sqrt{\pi_q^2a^2 - k_0^2a^2}}\left[\frac{a^2Z_1^2(\pi_q a)}{b^2Z_1^2(\pi_q b)} - 1\right] \tag{A46}$$

with

$$\gamma_{Bn} = \sqrt{\lambda_n^2 - k_0^2\varepsilon_1\mu_1} \tag{A39}$$

$$\gamma_{C_p} = \sqrt{\chi_p^2 - k_0^2\varepsilon_2\mu_2} \tag{A40}$$

and

$$\chi_p = \lambda_n, \qquad \text{for } n = p. \tag{A41}$$

Combining (A37) and (A38), the value of Γ_n is then found, as shown in (A42), at the top of this page. The unknowns x_m are found from (A26) if the integration of the quantity $rZ_1(\pi_m r)H_{\Phi B}$ is made between $r = b$ and $r = a$. The result is

$$\frac{Y_{Aq}}{2}A_q bZ_1(\pi_q b)\left[\frac{a^2Z_1^2(\pi_q a)}{b^2Z_1^2(\pi_q b)} - 1\right] = \sum_{n=1}^{\infty}\frac{Y_{Bn}B_n\lambda_n J_0(\lambda_n b)}{\lambda_n^2 - \pi_q^2}[1 - \Gamma_n]. \tag{A43}$$

If Y_{Aq}, Y_{Bn}, and B_n are substituted with (A5), (A12), and (A27) in (A43), it may be shown that

$$\frac{1}{4\varepsilon_1\sqrt{\pi_q^2a^2 - k_0^2a^2}}\frac{A_q}{A_0[1+\Gamma]}bZ_1(\pi_q b)\left[\frac{a^2Z_1^2(\pi_q a)}{b^2Z_1^2(\pi_q b)} - 1\right] = -\sum_{n-1}^{\infty}\frac{\lambda_n^2a^2}{(\lambda_n^2a^2 - \pi_q^2a^2)\sqrt{\lambda_n^2a^2 - k_0^2\varepsilon_1\mu_1a^2}}\frac{1-\Gamma_n}{1+\Gamma_n} \cdot \frac{J_0^2(\lambda_n b)}{J_1^2(\lambda_n a)}\left[1 - \sum_{m=1}^{\infty}\frac{A_m}{A_0(1+\Gamma)}\frac{bZ_1(\pi_m b)}{\pi_m^2a^2 - \lambda_n^2a^2}\right] \tag{A44}$$

or, most conveniently,

$$\sum_{m=1}^{\infty}A_{mq}x_m = y_q, \qquad q = 1, 2, \cdots \tag{A45}$$

by setting (A46), shown at the top of this page, where δ_{mq} is the Kronecker delta function and y_q is found by (A34).

Hence, the same procedure is adopted to calculate the admittance y_M (when a magnetic wall is placed at plane T). We have only to change in (A14)–(A16) and, consequently, in (A35)–(A38), sh function by ch function and ch function by sh function. Finally, we find the same results in replacing $\coth$ function with $\tanh$ function in (A42).

Appendix B
Inverse Problem

The iterative method used to calculate ε_i and μ_i (the constitutive parameters of the unknown layer) is derived from the gradient method.

For any initial vector

$$\vec{U}_0 = \begin{bmatrix}\varepsilon_i' \\ \varepsilon_i'' \\ \mu_i' \\ \mu_i''\end{bmatrix} \tag{B1}$$

we define an error vector $\Delta\vec{S}$ in the following manner:

$$\Delta\vec{S} = \begin{bmatrix}S_{11x}^{(m)} - S_{11x}^{(c)} \\ S_{11y}^{(m)} - S_{11y}^{(c)} \\ S_{21x}^{(m)} - S_{21x}^{(c)} \\ S_{21y}^{(m)} - S_{21y}^{(c)}\end{bmatrix} \tag{B2}$$

where the superscripts m and c denote, respectively, the measured and calculated S-parameters in rectangular coordinates.

At the $\Delta\vec{S}$ vector, we associate a second vector $\Delta\vec{U}$ as follows:

$$\Delta\vec{S} = [D]\Delta\vec{U} \tag{B3}$$

where the matrix $[D]$ is defined as the derivative matrix

$$[D] = \begin{bmatrix}\dfrac{\delta S_{11x}}{\delta\varepsilon_i'} & \dfrac{\delta S_{11x}}{\delta\varepsilon_i''} & \dfrac{\delta S_{11x}}{\delta\mu_i'} & \dfrac{\delta S_{11x}}{\delta\mu_i''} \\ \dfrac{\delta S_{11y}}{\delta\varepsilon_i'} & \dfrac{\delta S_{11y}}{\delta\varepsilon_i''} & \dfrac{\delta S_{11y}}{\delta\mu_i'} & \dfrac{\delta S_{11y}}{\delta\mu_i''} \\ \dfrac{\delta S_{21x}}{\delta\varepsilon_i'} & \dfrac{\delta S_{21x}}{\delta\varepsilon_i''} & \dfrac{\delta S_{21x}}{\delta\mu_i'} & \dfrac{\delta S_{21x}}{\delta\mu_i''} \\ \dfrac{\delta S_{21y}}{\delta\varepsilon_i'} & \dfrac{\delta S_{21y}}{\delta\varepsilon_i''} & \dfrac{\delta S_{21y}}{\delta\mu_i'} & \dfrac{\delta S_{21y}}{\delta\mu_i''}\end{bmatrix} \tag{B4}$$

and

$$\Delta\vec{U} = \begin{bmatrix}\Delta\varepsilon_i' \\ \Delta\varepsilon_i'' \\ \Delta\mu_i' \\ \Delta\mu_i''\end{bmatrix}. \tag{B5}$$

The value of the $\Delta\vec{U}$ vector is obtained from the inverse matrix $[D]^{-1}$ as follows:

$$\Delta\vec{U} = [D]^{-1} \cdot \Delta\vec{S}. \tag{B6}$$

The nth direction of investigation is now

$$\vec{U}_n = \vec{U}_{n-1} + \begin{bmatrix} \alpha_1 \Delta\varepsilon_i' \\ \alpha_2 \Delta\varepsilon_i' \\ \alpha_3 \Delta\mu_i' \\ \alpha_4 \Delta\mu_i'' \end{bmatrix} \tag{B7}$$

where the α_j coefficients are less than 0.9. The calculated (ε_i, μ_i) values become the initial values for the next measured point. The iterations are stopped when $||\Delta\vec{S}||^2$ is lower than 10^{-8}. The typical computation time for 201 frequency measured points is 1 min using an HP 715-75 workstation.

REFERENCES

[1] N. E. Belhadj-Tahar and A. Fourrier-Lamer, "Broad-band analysis of a coaxial discontinuity used for dielectric measurements," *IEEE Trans. Microwave Theory Tech.*, vol. MTT-34, pp. 346–350, Mar. 1986.

[2] N. E. Belhadj-Tahar, O. Meyer, and A. Fourrier-Lamer, "Broad-band microwave characterization of bilayered materials using a coaxial discontinuity with applications for thin conductive films for microelectronics and material in airtight cell," *IEEE Trans. Microwave Theory Tech.*, vol. 45, pp. 260–267, Feb. 1997.

[3] N. E. Belhadj-Tahar, A. Fourrier-Lamer, and H. de Chanterac, "Broad-band simultaneous measurement of complex permittivity and permeability using a coaxial discontinuity," *IEEE Trans. Microwave Theory Tech.*, vol. 38, pp. 1–7, Jan. 1990.

[4] N. E. Belhadj-Tahar and A. Fourrier-Lamer, "Broad-band simultaneous measurement of the complex permittivity tensor for uniaxial materials using a coaxial discontinuity," *IEEE Trans. Microwave Theory Tech.*, vol. 39, pp. 1718–1724, Oct. 1991.

[5] W. B. Weir, "Automatic measurement of complex dielectric constant and permeability at microwave frequencies," *Proc. IEEE*, vol. 62, pp. 33–36, Jan. 1974.

[6] F. Buckley and A. A. Maryott, "Tables of dielectric dispersion data for pure liquids and dilute solutions," in *Circular 589*. Washington, DC: National Bureau of Standards, 1958.

[7] O. Dubrunfaut, "Instrumentation pour la caractérisation aux fréquences micro-ondes de matériaux magnétiques solides ou liquides," Thèse de l'Université Pierre et Marie Curie, Paris, France, Oct. 1997.

[8] R. Massart, "Preparation of aqueous magnetic liquids in alkaline and acidic media," *IEEE Trans. Magn.*, vol. MAG-17, pp. 1247–1248, Mar. 1981.

[9] C. Kittel, "On the theory of ferromagnetic resonance absorption," *Phys. Rev.*, vol. 73, pp. 155–161, Feb. 1948.

Nour-eddine Belhadj-Tahar received the Doctorat degree in electrical engineering and Habilitation à Diriger les Recherches degree from the University Pierre et Marie Curie, Paris, France, in 1986 and 1997, respectively.

He is currently Maître de Conférences at the University Pierre et Marie Curie. His current research activities include electromagnetic-wave propagation in waveguide structures and applications of discontinuities for microwave and millimeter-wave materials characterization.

Olivier Dubrunfaut received the Doctorat degree in electrical engineering from the Université Pierre et Marie Curie, Paris, France, in 1997.

He is currently an Assistant Professor (Attaché Temporaire d'Enseignement et de Recherche) at the University Pierre et Marie Curie. His research has dealt with microwave dielectric and magnetic measurement technique.

Arlette Fourrier-Lamer received the Doctorat d'Etat ès Sciences Physiques degree from the University Pierre et Marie Curie, Paris, France, in 1981.

She is currently a Professor of electronic engineering at the University Pierre et Marie Curie. Until 1981, she was engaged in research on electronic and nuclear double resonance (ENDOR) in paramagnetic liquids. Since 1982, she has been working on electromagnetic discontinuities and applications to materials characterization (resins, conducting polymers, superconductors, and ferrites). Her current areas of interest include nonlinear electromagnetics, wave propagation in chiral media, and microwave processing.